HHS Public Access

Author manuscript

Radiat Res. Author manuscript; available in PMC 2022 November 01.

Published in final edited form as:

Radiat Res. 2021 November 01; 197(3): 0. doi:10.1667/RADE-21-00166.1.

Sensitization of endothelial cells to ionizing radiation exacerbates delayed radiation myelopathy in mice

Chang-Lung Lee[1,2], **Ato O. Wright**[1], **Jessica W. Lee**[1], **Jeremy Brownstein**[1], **Stephanie Hasapis**[1], **Sloane Satow**[1], **Lorraine Da Silva Campos**[1], **Nerissa Williams**[1], **Yan Ma**[1], **Lixia Luo**[1], **Timothy Johnson**[1], **Andrea R. Daniel**[1], **William T. Harrison**[4], **Mark Oldham**[1], **David G. Kirsch**[1,3]

[1]Department of Radiation Oncology, Duke University Medical Center, Durham, North Carolina 27710, USA.

[2]Department of Pathology, Duke University Medical Center, Durham, North Carolina 27710, USA.

[3]Department of Pharmacology & Cancer Biology, Duke University Medical Center, Durham, North Carolina 27710, USA.

[4]Department of Pathology, Wake Forest Baptist Health, Winston Salem, North Carolina 27157, USA.

Abstract

Delayed radiation myelopathy is a rare, but significant late side effect from radiation therapy that can lead to paralysis. The cellular and molecular mechanisms leading to delayed radiation myelopathy are not completely understood, but may be a consequence of damage to oligodendrocyte progenitor cells and vascular endothelial cells. Here, we aimed to determine the contribution of endothelial cell damage to the development of radiation-induced spinal cord injury using a genetically defined mouse model in which endothelial cells are sensitized to radiation due to loss of the tumor suppressor p53. Tie2Cre; $p53^{FL/+}$ and Tie2Cre; $p53^{FL/-}$ mice, which lack one and both alleles of p53 in endothelial cells, respectively, were treated with focal irradiation that specifically targeted the lumbosacral region of the spinal cord. The development of hindlimb paralysis was followed for up to 18 weeks after a single fraction of 26.7 Gy or 28.4 Gy. During 18 weeks of follow-up, 83% and 100% of Tie2Cre; $p53^{FL/-}$ mice developed hindlimb paralysis after 26.7 and 28.4 Gy, respectively. In contrast, during this period only 8% of Tie2Cre; $p53^{FL/+}$ mice exhibited paralysis after 28.4 Gy. In addition, 8 weeks after 28.4 Gy the irradiated spinal cord from Tie2Cre; $p53^{FL/-}$ mice showed a significantly higher fractional area positive for the neurological injury marker glial fibrillary acidic protein (GFAP) compared with the irradiated spinal cord from Tie2Cre; $p53^{FL/+}$ mice. Together, our findings show that deletion of p53 in endothelial cells

CORRESPONDENCE David G. Kirsch, Duke University Medical Center, Box 91006, Durham, NC 27708, Phone: 919-681-8605, Fax: 919-681-1867, david.kirsch@duke.edu.

CONFLICT OF INTEREST

DGK is on the scientific advisory board and owns stock in Lumicell, Inc which is developing intraoperative imaging technology. DGK is a co-founder of X-RAD Therapeutics, which is developing radiosensitizers. DGK reports research support from Merck, Bristol Myers Squibb, Varian, and X-RAD Therapeutics. C-LL reports research support from Janssen R&D and Rythera Therapeutics. None of these interests present a conflict with the content in this manuscript. The remaining authors have no conflicting financial interests.

sensitizes mice to the development of delayed radiation myelopathy indicating that endothelial cells are a critical cellular target of radiation that regulates myelopathy.

INTRODUCTION

Radiation myelopathy is a rare but severe late toxicity of radiation exposure to the spinal cord. The clinical latency period is usually at least 6 months, with one series reporting a mean latency of 18.5 months after radiation therapy (1). The neurologic deficits are typically progressive and irreversible, ranging from minor paresthesia to Brown-Sequard syndrome with paralysis (2). Factors affecting the risk of radiation myelopathy include dose-fractionation, volume of spinal cord irradiated, and dose rate. For example, a QUANTEC review reported a <0.2% risk following 50 Gy in 25 fractions to the full cord and <1% risk following 13 Gy single fraction to the partial cord (3). Animal studies have reported an ED_{50}, or dose causing paralysis in 50% of animals, ranging from approximately 20 to 90 Gy in a single fraction depending on the volume of the spinal cord irradiated (4).

The pathogenesis of late radiation myelopathy has been suggested to be caused by white matter necrosis due to cell death of oligodendrocyte progenitor cells (OPCs) and/or vascular endothelial cells (5,6). In a boron neutron capture therapy study in rats where radiation was delivered preferentially to the vasculature, injury of endothelial cells rather than OPCs appeared to be the primary cause of white matter necrosis (5,7). However, it is not clear if endothelial cell damage is sufficient to cause radiation-induced myelopathy (8,9).

The goal of this study is to define the role of endothelial cell damage in regulating radiation-induced myelopathy by using genetically engineered mice in which endothelial cells are sensitized to radiation due to the loss of the tumor suppressor p53 (10-13). We previously defined an essential role for p53 in protecting cardiac endothelial cells from radiation (10). We observed that deletion of both alleles of p53 in endothelial cells sensitizes mice to myocardial injury and delayed gastrointestinal injury following whole heart and whole abdominal irradiation, respectively (10,13). Here, we applied this genetically defined model to investigate the role of endothelial cell injury in regulating myelopathy following a single fraction of focal spinal irradiation.

MATERIALS AND METHODS

Experimental animals.

Animal procedures were approved by the Institutional Animal Care and Use Committee at Duke University. Animal experiments were conducted using 8 to 12 week old Tie2Cre; $p53^{FL/-}$ mice and Tie2Cre; $p53^{FL/+}$ littermates, which have been characterized previously (10). Both males and females were used in the study (Supplementary Table 1). Mouse genotyping was performed by Transnetyx (Cordova, TN). The development of hindlimb paralysis was examined by a rotarod performance test every two weeks. Mice were defined as paralyzed if they that had riding time less than 60 seconds on a rotating rotarod apparatus (Supplementary Video 1) or showed clinically apparent hindlimb paralysis.

Radiation treatment.

Spinal cord irradiation was performed using a small animal irradiator, X-RAD 225Cx (Precision X-Ray). The commissioning of this machine and the accuracy of image guided radiation treatment delivery was described previously (14,15). Prior to irradiation, mice received isoflurane anesthesia and were positioned supine on the treatment stage. The spinal treatment plan consisted of a single 180-degree arc, which began with the beam entering laterally on the left side of the supine mouse (90-degree gantry angle) and proceeding clockwise with the beam moving under the couch to finish entering laterally on the right side of the mouse (270-degree gantry angle). The isocenter was placed in the lumbosacral spine with onboard fluoroscopy using 40 kVp (2.5 mA) X-rays and a 2 mm Al imaging filter. Radiation to the spine was delivered with 225 kVp (13 mA) X-rays and a 3 mm Cu treatment filter. The beam was collimated with a Cu portal yielding an 8x12 mm rectangular field. The dose rate at isocenter was estimated to be 2.84 ± 0.39 Gy/min, which was assessed by Gafchromic EBT film measurement in a simplified geometry as illustrated in Figure 1. The bean-on time of 564 seconds and 600 seconds was used to deliver 26.7 Gy and 28.4 Gy, respectively.

Histology.

Mice were euthanized by CO_2 asphyxiation before tissue collection. Spinal cord was harvested using an ejection method described previously (16). To prepare paraffin-embedded tissues, tissues specimens were fixed in 10% neutralized formalin overnight, preserved in 70% ethanol, and then cut into 6 pieces before being embedded in paraffin. For immunohistochemistry (IHC) staining, sections cut from paraffin embedded tissues were deparaffinized with xylene and rehydrated with a graded series of ethanol and water washes. Antigen retrieval was performed by a Citrate-based Antigen Unmasking Solution (Vector Laboratories, H-3300-250) followed by staining with an anti-glial fibrillary acidic protein (GFAP) antibody (Agilent Dako, Z0334) or an anti-Phospho-Histone H2A.X (Ser139) (gamma-H2AX) antibody (Cell Signaling Technologies #9718). Corresponding secondary antibodies (Vector Laboratories) were used according to manufacturer's instruction. The staining signal was developed using VECTASTAIN Elite ABC reagent in combination with Vector DAB Substrate (Vector Laboratories).

To quantify the area of the spinal cord stained positive for GFAP, images of lumbosacral sections were acquired at 5x magnification to capture the entire section. An in-house MATLAB image segmentation script was used to measure the total area of each spinal cord section and the area of each spinal cord section stained positive for GFAP. Quantification was conducted by a single observer (S.S.) blinded to the genotype.

Statistical considerations.

Kaplan–Meier estimate was performed followed by the log-rank test. Pairwise comparisons of quantitative phenotypes were based on the Mann-Whitney U test. Data are presented as mean ± SEM and each data point represents one mouse. We considered the evidence against a null hypothesis to be significant if the unadjusted p-value for the corresponding test was less than 0.05. GraphPad Prism 9 (GraphPad Software, Inc.) was used for carrying out these statistical analyses.

RESULTS

To focally irradiate the spinal cord while minimizing dose to nearby normal tissues, we used a single 180-degree arc to deliver X-rays targeting an 8x12 mm rectangular field of the lumbosacral region of the spinal cord. The spinal cord volume was contoured on a representative CT, and a representative dose-volume histogram is shown in Figure 2A. The treated volume included approximately 20% of the spinal cord and excluded most of the surrounding organs including the kidneys, liver, bladder, and small bowel (Figure 2, A and B). To validate the precision of spinal cord irradiation, we stained the spinal cord harvested 30 minutes after 26.7 Gy with a DNA damage marker gamma-H2AX. We observed substantially stronger gamma-H2AX staining on the tissue sections inside the irradiation field compared with the tissue sections outside the irradiation field (Figure 2C). Collectively, these results demonstrate that the treatment plan precisely irradiates a small volume of the murine spinal cord to study radiation-induced myelopathy.

To determine the impact of endothelial cell injury on the formation of radiation-induced myelopathy, we delivered either 26.7 Gy or 28.4 Gy X-rays to the spinal cord of Tie2Cre; $p53^{FL/-}$ mice, which lack both alleles of p53 in endothelial cells, and Tie2Cre; $p53^{FL/+}$ mice, which retain one functional allele of p53 in endothelial cells. These radiation doses were selected based on results from published preclinical studies that examine spinal cord tolerance to radiation in research animals (4). None of the irradiated mice showed mortality within 30 days after irradiation due to the acute radiation syndrome (Figure 3A). Mice were followed for the development of hindlimb paralysis for up to 18 weeks after irradiation. This follow-up time was chosen because Tie2Cre; $p53^{FL/-}$ mice can start to develop thymic lymphoma as both alleles of p53 are also deleted in the majority of hematopoietic cells by Tie2Cre (10,17). We observed that the incidence of radiation-induced hindlimb paralysis was significantly higher in Tie2Cre; $p53^{FL/-}$ mice compared with Tie2Cre; $p53^{FL/+}$ mice following both 26.7 Gy and 28.4 Gy (Figure 3A). The incidence of paralysis after 26.7 Gy was 83% (10 out of 12) for Tie2Cre; $p53^{FL/-}$ mice and 0% (0 out of 8) for Tie2Cre; $p53^{FL/+}$ mice, while the incidence of paralysis after 28.4 Gy was 100% (9 out of 9) for Tie2Cre; $p53^{FL/-}$ mice and 8% (1 out of 12) for Tie2Cre; $p53^{FL/+}$ mice. No statistically significant difference in paralysis-free survival was observed between male and female Tie2Cre; $p53^{FL/-}$ mice after either 26.7 or 28.4 Gy (Supplementary Figure 1).

Examination of mice that developed paralysis showed that spinal cord sections from the lumbosacral region exhibited neuronal loss and gliosis within the anterior horns of the spinal cord, while the neurons within the dorsal horns were relatively unaffected (Figure 3B). In addition, we examined reactive astrogliosis, a process in which astrocytes respond to injury in the central nervous system, in the lumbosacral spinal cord from Tie2Cre; $p53^{FL/-}$ and Tie2Cre; $p53^{FL/+}$ mice 8 weeks after 28.4 Gy by staining with GFAP, a classic marker for reactive astrocytes (18,19). Our results showed a substantial increase in GFAP+ cells in the lumbosacral spinal cord from irradiated mice compared to unirradiated controls (Figure 3C). Moreover, the GFAP+ fractional area was significantly higher in the lumbosacral spinal cord of irradiated Tie2Cre; $p53^{FL/-}$ mice compared with irradiated Tie2Cre; $p53^{FL/+}$ mice 8 weeks after 28.4 Gy (Figure 3D). Together, our results demonstrate that sensitization of endothelial cells to radiation promotes delayed radiation myelopathy in mice.

DISCUSSION

Both OPCs and endothelial cells have been implicated in the pathogenesis of radiation myelopathy. In rat models, <1% of OPCs survive within 6 weeks following a single 15-40 Gy fraction to the spinal cord (8,20). Dose-dependent recovery and a second decline in OPCs has also been observed at 12 weeks and 4-5 months after radiation, respectively (8). Interestingly, OPCs of mice may be more radioresistant as 30-35% OPCs survive weeks following 40 Gy to the spinal cord in adult C57BL/6J mice (20). One study in rats suggested that cell death of oligodendrocytes may not initiate late radiation myelopathy because a decrease in oligodendrocyte density was observed at 24 hours and up to 20 weeks following both a non-paralytic dose of 8 Gy and a paralytic dose of 22 Gy (21). On the other hand, pathologic studies in rats using a single fraction of 25-30 Gy showed significant endothelial cell loss and disruption of the blood-spinal cord barrier at 14-90 days after radiation, which preceded white matter changes and neurologic deficits (22,23). In addition, the aforementioned boron neutron capture study also provided evidence indicating that endothelial cell loss is the primary driver that initiates radiation myelopathy (7).

Other investigators have previously reported the role of p53 in regulating the pathologic changes of the spinal cord 24 hours after irradiation. For example, one study showed that 22 Gy irradiation to the spinal cord of $p53^{+/+}$ mice resulted in apoptosis of oligodendrocytes at 24 hours (24). This apoptotic response was absent in $p53^{-/-}$ mice, suggesting that p53 is necessary to cause early oligodendrocyte apoptosis following irradiation. On the other hand, early radiation-induced apoptosis of endothelial cells appears to rely on the acid sphingomyelinase (ASMase) pathway instead of p53 (24-26). A previous study in mice reported that following 50 Gy radiation to the spinal cord, $ASMase^{+/+}$, $p53^{+/+}$, and $p53^{-/-}$ mice all exhibited a similar degree of endothelial cell loss and blood-spinal cord barrier disruption, while $ASMase^{-/-}$ mice were reported to show preserved endothelial cell number with no blood-spinal cord barrier leakage (26). In contrast to the above studies, which were conducted at 24 hours following radiation to study early radiation injury of the spinal cord, results from our experiments that examined paralysis of Tie2Cre; $p53^{FL/-}$ and Tie2Cre; $p53^{FL/+}$ mice following spinal cord irradiation demonstrate that deletion of both alleles of p53 in endothelial cells is sufficient to sensitize mice to delayed radiation myelopathy.

To focally irradiate the spinal cord, we utilized a 180-degree arc treatment plan that minimizes radiation dose to surrounding normal tissues including the kidneys, liver, bladder, and small bowel compared with the parallel-opposed beams typically employed in animal models. To estimate the radiation dose delivered by arc treatment to the isocentric point, we developed a novel approach to perform dosimetry using Gafchromic EBT film measurement in a simplified geometry. The advantage of this set-up is that any uncertainties associated with angular dependency of EBT film response is removed from the measurement. There are several uncertainties in this dose measurement, including the assumption of a water equivalent mouse, the estimation of the average separation along the arc, the variability between mice, isocenter placement between mice, and uncertainties in calibrating EBT3 film. Nevertheless, our approach provides a novel and straightforward way to conduct dosimetry of arc radiation treatment for small animal studies.

This study has several limitations. First, mice were only followed for up to 18 weeks after irradiation. Therefore, it is not clear whether sensitization of endothelial cells to radiation would also increase the overall incidence of radiation-induced myelopathy because Tie2Cre; $p53^{FL/+}$ littermate controls could develop hindlimb paralysis months later (4). Second, Tie2Cre causes recombination of the p53 allele in both endothelial cells and hematopoietic cells (10). Because deletion of p53 in hematopoietic cells augments inflammatory responses due to the loss of p53-mediated NF-κB suppression (27), it is possible that enhanced tissue inflammation also contributes to the phenotype of accelerated radiation-induced myelopathy that we observed in Tie2Cre; $p53^{FL/-}$ mice. Nevertheless, our results in this study have established a robust mouse model that we can use to investigate the role of endothelial cells in regulating the spinal cord tolerance and the alpha/beta ratio of the spinal cord in the future.

In sum, our results demonstrate that mice in which both alleles of p53 are deleted in endothelial cells are sensitized to delayed radiation myelopathy. This observation is consistent with our previously published studies showing that deletion of p53 in endothelial cells promotes the development of radiation-induced myocardial injury (10) and radiation-induced delayed intestinal injury (13). Together, these findings demonstrate that p53 functions in endothelial cells to prevent the development of radiation-induced late effects in multiple organs.

Supplementary Material

Refer to Web version on PubMed Central for supplementary material.

ACKNOWLEDGEMENTS

This work was supported by National Cancer Institute grant R35 CA197616 (D.G.K) and the Whitehead Scholar Award from Duke University School of Medicine (C-L.L).

REFERENCES

1. Wong CS, Van Dyk J, Milosevic M, Laperriere NJ. Radiation myelopathy following single courses of radiotherapy and retreatment. Int J Radiat Oncol Biol Phys. 1994;30(3):575–81. [PubMed: 7928488]
2. Schultheiss TE, Kun LE, Ang KK, Stephens LC. Radiation response of the central nervous system. Int J Radiat Oncol Biol Phys. 1995;31(5):1093–112. [PubMed: 7677836]
3. Kirkpatrick JP, van der Kogel AJ, Schultheiss TE. Radiation dose-volume effects in the spinal cord. Int J Radiat Oncol Biol Phys. 2010;76(3 Suppl):S42–9. [PubMed: 20171517]
4. Medin PM, Boike TP. Spinal cord tolerance in the age of spinal radiosurgery: lessons from preclinical studies. Int J Radiat Oncol Biol Phys. 2011;79(5):1302–9. [PubMed: 21183290]
5. Wong CS, Fehlings MG, Sahgal A. Pathobiology of radiation myelopathy and strategies to mitigate injury. Spinal Cord. 2015 8;53(8):574–80. [PubMed: 25800695]
6. Okada S, Okeda R. Pathology of radiation myelopathy. Neuropathology. 2001;21(4):247–65. [PubMed: 11837531]
7. Coderre JA, Morris GM, Micca PL, Hopewell JW, Verhagen I, Kleiboer BJ, et al. Late effects of radiation on the central nervous system: role of vascular endothelial damage and glial stem cell survival. Radiat Res. 2006 9;166(3):495–503. [PubMed: 16953668]
8. Wong CS, Van der Kogel AJ. Mechanisms of radiation injury to the central nervous system: implications for neuroprotection. Mol Interv. 2004;4(5):273–84. [PubMed: 15471910]

9. Kim JH, Brown SL, Jenrow KA, Ryu S. Mechanisms of radiation-induced brain toxicity and implications for future clinical trials. J Neurooncol. 2008;87(3):279–86. [PubMed: 18209952]
10. Lee CL, Moding EJ, Cuneo KC, Li Y, Sullivan JM, Mao L, et al. p53 functions in endothelial cells to prevent radiation-induced myocardial injury in mice. Sci Signal. 2012;5(234):ra52. [PubMed: 22827996]
11. Lee C-L, Blum JM, Kirsch DG. Role of p53 in regulating tissue response to radiation by mechanisms independent of apoptosis. Transl Cancer Res. 2013 10;2(5):412–21. [PubMed: 24466508]
12. Lee CL, Min H, Befera N, Clark D, Qi Y, Das S, et al. Assessing Cardiac Injury in Mice With Dual Energy-MicroCT, 4D-MicroCT, and MicroSPECT Imaging After Partial Heart Irradiation. Int J Radiat Oncol Biol Phys. 2014;88(3):686–93. [PubMed: 24521682]
13. Lee C-L, Daniel AR, Holbrook M, Brownstein J, Silva Campos LD, Hasapis S, et al. Sensitization of Vascular Endothelial Cells to Ionizing Radiation Promotes the Development of Delayed Intestinal Injury in Mice. Radiat Res. 2019 9;192(3):258–66. [PubMed: 31265788]
14. Newton J, Oldham M, Thomas A, Li Y, Adamovics J, Kirsch DG, et al. Commissioning a small-field biological irradiator using point, 2D, and 3D dosimetry techniques. Med Phys. 2011 12;38(12):6754–62. [PubMed: 22149857]
15. Rankine LJ, Newton J, Bache ST, Das SK, Adamovics J, Kirsch DG, et al. Investigating end-to-end accuracy of image guided radiation treatment delivery using a micro-irradiator. Phys Med Biol. 2013 11 7;58(21):7791–801. [PubMed: 24140983]
16. Kennedy HS, Jones C 3rd, Caplazi P. Comparison of standard laminectomy with an optimized ejection method for the removal of spinal cords from rats and mice. J Histotechnol. 2013;36(3):86–91. [PubMed: 24039319]
17. Lee C-L, Brock KD, Hasapis S, Zhang D, Sibley AB, Qin X, et al. Whole exome sequencing of radiation-induced thymic lymphoma in mouse models identifies Notch1 activation as a driver of p53 wild-type lymphoma. Cancer Res [Internet]. 2021 5 25; Available from: 10.1158/0008-5472.CAN-20-2823
18. Eng LF, Ghirnikar RS. GFAP and astrogliosis. Brain Pathol. 1994 7;4(3):229–37. [PubMed: 7952264]
19. Zamanian JL, Xu L, Foo LC, Nouri N, Zhou L, Giffard RG, et al. Genomic analysis of reactive astrogliosis. J Neurosci. 2012 5 2;32(18):6391–410. [PubMed: 22553043]
20. Chari DM, Huang WL, Blakemore WF. Dysfunctional oligodendrocyte progenitor cell (OPC) populations may inhibit repopulation of OPC depleted tissue. J Neurosci Res. 2003;73(6):787–93. [PubMed: 12949904]
21. Atkinson S, Li YQ, Wong CS. Changes in oligodendrocytes and myelin gene expression after radiation in the rodent spinal cord. Int J Radiat Oncol Biol Phys. 2003;57(4):1093–100. [PubMed: 14575841]
22. Stewart PA, Vinters HV, Wong CS. Blood-spinal cord barrier function and morphometry after single doses of x-rays in rat spinal cord. Int J Radiat Oncol Biol Phys. 1995;32(3):703–11. [PubMed: 7790257]
23. Zhang J, Wei L, Sun WL, Wang L, Zhang WJ, You H. Radiation-induced endothelial cell loss and reduction of the relative magnitude of the blood flow in the rat spinal cord. Brain Res. 2014;1583:193–200. [PubMed: 24953932]
24. Chow BM, Li YQ, Wong CS. Radiation-induced apoptosis in the adult central nervous system is p53-dependent. Cell Death Differ. 2000;7(8):712–20. [PubMed: 10918445]
25. Santana P, Pena LA, Haimovitz-Friedman A, Martin S, Green D, McLoughlin M, et al. Acid sphingomyelinase-deficient human lymphoblasts and mice are defective in radiation-induced apoptosis. Cell. 1996;86(2):189–99. [PubMed: 8706124]
26. Li YQ, Chen P, Haimovitz-Friedman A, Reilly RM, Wong CS. Endothelial apoptosis initiates acute blood-brain barrier disruption after ionizing radiation. Cancer Res. 2003;63(18):5950–6. [PubMed: 14522921]
27. Gudkov AV, Gurova KV, Komarova EA. Inflammation and p53: A tale of two stresses. Genes Cancer. 2011 4;2(4):503–16. [PubMed: 21779518]

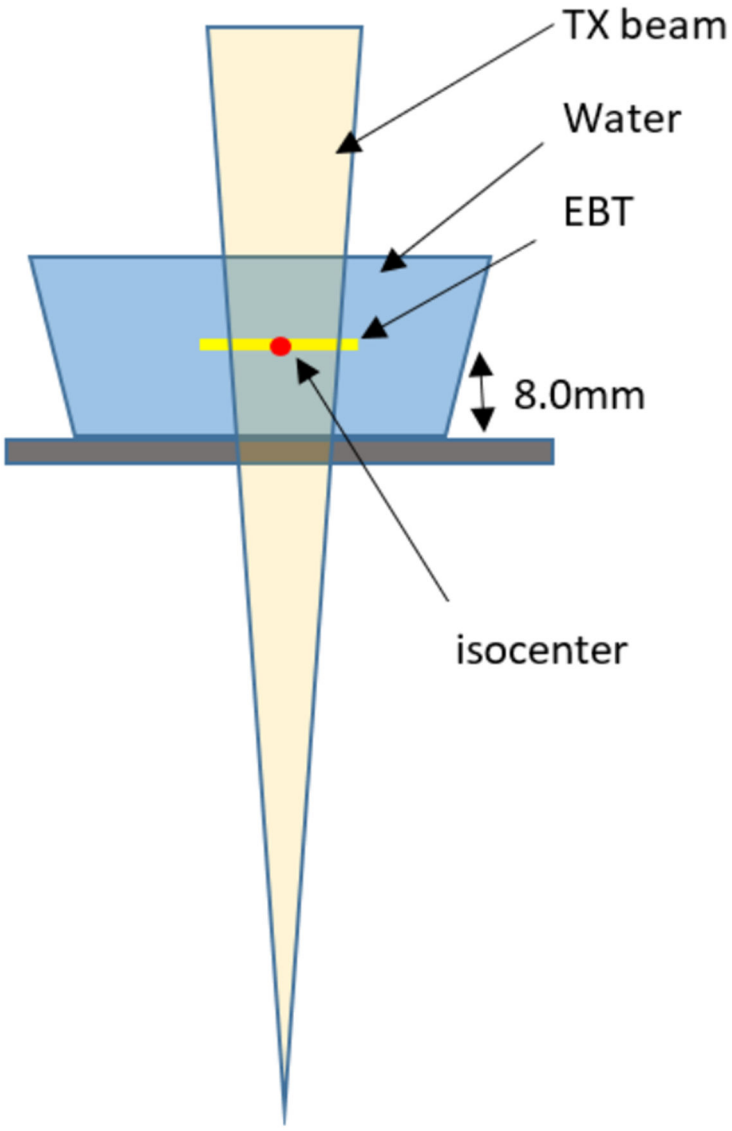

Figure 1. Estimation of the radiation dose delivered to the spinal cord.

The delivered dose to the isocentric point (positioned on the spinal cord) was estimated by Gafchromic EBT film measurement in a simplified geometry. The average separation along the arc was calculated to be 8.0±0.5mm from the planning CT data (i.e. the average skin-to-isocenter distance). A small water phantom was then constructed with a 3D printed slot to hold a 40x40mm piece of EBT3 film at exactly 8.0mm up from the base of the water bath. The treatment delivery was then given to the phantom (isocenter placed on the film) in the exact same way as to the mouse, except that the gantry was fixed at 180 degrees for the entire duration of irradiation.

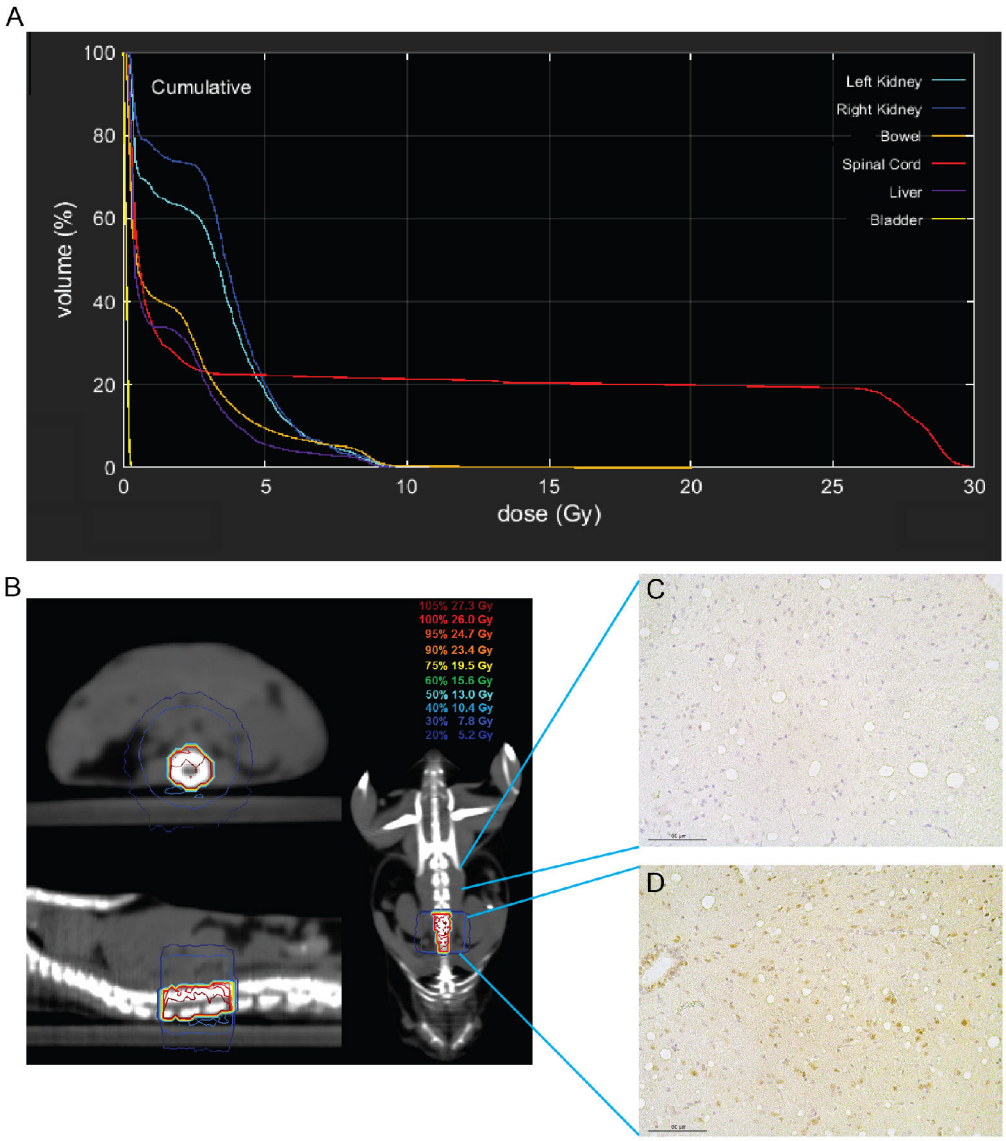

Figure 2.

Treatment plan for murine spinal cord irradiation. **(A)** Dose-volume metrics of the spinal cord for a single dose of 26.7 Gy focal irradiation. **(B)** Prescription isodose lines on a representative CT in the axial (top left), sagittal (bottom left), and coronal (right) planes. **(C and D)** Immunohistochemistry staining for gamma-H2AX, a biomarker for DNA double-strand breaks, on tissue sections of the spinal cord from unirradiated (C) and irradiated (D) areas of the same mouse. Scale bar represents 100 μm.

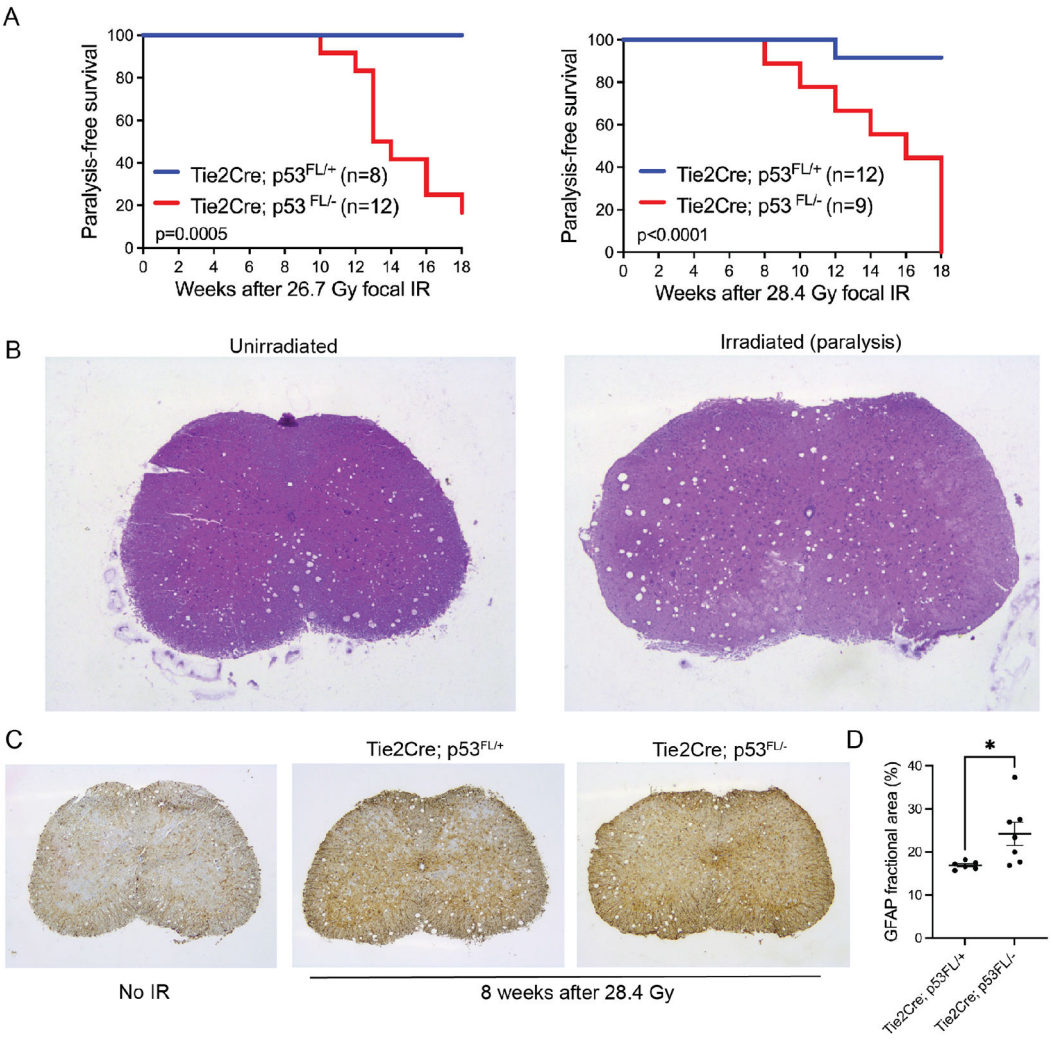

Figure 3.

Survival and histology of mice that received focal irradiation to the spinal cord. **(A)** Kaplan-Meier survival analysis of Tie2Cre; $p53^{FL/+}$ and Tie2Cre; $p53^{FL/-}$ mice after a single fraction of 26.7 Gy or 28.4 Gy spinal cord irradiation. P-value was calculated by log-rank test. **(B)** Representative images of H&E-stained lumbar section of the spinal cord from a Tie2Cre; $p53^{FL/-}$ mouse without irradiation (No IR) or a Tie2Cre; $p53^{FL/-}$ mouse that developed hindlimb paralysis 8 weeks following 28.4 Gy. **(C)** Representative images of immunohistochemistry staining of GFAP, a marker for reactive astrocytes, on the lumbar section of the spinal cord from mice without irradiation (No IR) or 8 weeks after 28.4 Gy. **(D)** Quantification of the lumbar section of the spinal cord stained with GFAP. The spinal cord was harvested from Tie2Cre; $p53^{FL/+}$ and Tie2Cre; $p53^{FL/-}$ mice 8 weeks after 28.4 Gy. The GFAP fractional area was calculated as the area stained positive for GFAP over the total area of the spinal cord. Data are presented as mean ± SEM. Each dot represents one mouse. *p<0.05 by Mann-Whitney U test.